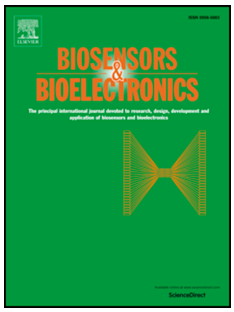

Target-driven rolling walker based electrochemical biosensor for ultrasensitive detection of circulating tumor DNA using doxorubicin@tetrahedron-Au tags

Dandan Li, Yixin Xu, Lu Fan, Bo Shen, Xiaojuan Ding, Rui Yuan, Xinmin Li, Weixian Chen

PII: S0956-5663(19)30905-4

DOI: https://doi.org/10.1016/j.bios.2019.111826

Reference: BIOS 111826

To appear in: *Biosensors and Bioelectronics*

Received Date: 14 August 2019

Revised Date: 5 October 2019

Accepted Date: 25 October 2019

Please cite this article as: Li, D., Xu, Y., Fan, L., Shen, B., Ding, X., Yuan, R., Li, X., Chen, W., Target-driven rolling walker based electrochemical biosensor for ultrasensitive detection of circulating tumor DNA using doxorubicin@tetrahedron-Au tags, *Biosensors and Bioelectronics* (2019), doi: https://doi.org/10.1016/j.bios.2019.111826.

CRediT author statement

Dandan Li: Conceptualization, Methodology, Software, Writing- Reviewing and Editing. **Yixin Xu:** Data curation, Writing- Original draft preparation. **Lu Fan:** Software. **Bo Shen:** Visualization. **Xiaojuan Ding**: Investigation. **Rui Yuan**: Methodology. **Xinmin Li:** Conceptualization, Writing- Reviewing and Editing, Supervision. **Weixian Chen**: Data curation, Validation.

Target-driven rolling walker based electrochemical biosensor for ultrasensitive detection of circulating tumor DNA using doxorubicin@tetrahedron-Au tags

Dandan Li[a,1], Yixin Xu[a,1], Lu Fan[b], Bo Shen[c], Xiaojuan Ding[a], Rui Yuan[d], Xinmin Li[c,*], Weixian Chen[a,*]

[a] *Department of Laboratory Medicine, The Second Affiliated Hospital of Chongqing Medical University, Chongqing 400010, China*

[b] *Key Laboratory of Clinical Laboratory Diagnostics (Ministry of Education), College of Laboratory Medicine, Chongqing Medical University, Chongqing 400016, China*

[c] *Department of Laboratory Medicine, Chongqing Traditional Chinese Medicine Hospital, Chongqing, Chongqing 400011, China*

[d] *Key Laboratory for Biorheological Science and Technology of Ministry of Education, State and Local Joint Engineering Laboratory for Vascular Implants, Bioengineering College of Chongqing University, Chongqing, 400044, China*

* Corresponding author. Tel: +86- 23-63703244; Fax: +86-23-63703244.

E-mail: xinmnli@163.com (X. M. Li) and chenweixian75@163.com (W. X. Chen)

[1] These authors contributed equally to this work.

Abstract

In this study, a multiple-legged and highly integrated DNA rolling walker based electrochemical biosensor was developed for ultrasensitive ctDNA analysis through rolling circle amplification (RCA) with doxorubicin@tetrahedron-Au (DOX@TDN-Au) as electrochemical indicator. Upon target-driven RCA, the multiple-legged walker could move along with the predesigned track by strand displacement reactions, resulting in numbers of legs binding irreversibly to iStep probes. The binding of massive legs to iStep probes could effectively impede DOX@TDN-Au tags binding on the surface of sensor and then reached a "signal off" state. Benefiting from the highly amplified efficiency of rolling walker machine and DOX@TDN-Au tags, the established biosensor performed high sensitivity for target detection with a low limit of detection down to 0.29 fM. Moreover, the target ctDNA could hybridize with the ring and capture probe simultaneously, greatly enhancing the specificity of the developed biosensing method. Thus, this biosensing method is a promising tool for detection of ctDNA in the field of clinical diagnostic and tumor progression assessment.

Keywords: Circulating tumor DNA; Rolling walker; Rolling circle amplification; Doxorubicin-tetrahedron; Electrochemistry

1. Introduction

Circulating tumor DNA (ctDNA) is a single-stranded or double-stranded gene fragments originating from tumor or circulating tumor cells, and subsequently released to peripheral blood (Chan et al., 2013; Speicher and Pantel, 2014). Studies have shown that ctDNA is a potential tumor biomarker which has gained increasing attentions in term of cancer assessment (Koldby et al., 2019; Sumbal et al., 2018). For example, kirsten rat sarcoma-2 virus (kras) point mutations are closely related to different cancers including lung cancer, colorectal cancer, and ovarian cancer (Kamerkar et al., 2017). Thus, quantitative analysis of ctDNA plays a vital role in clinical diagnosis, tumor progress and cancer recurrence (Gorgannezhad et al., 2018; Li et al., 2019).

Currently, the routine methods for ctDNA analysis are polymerase chain reaction (PCR) and DNA sequencing (Das et al., 2016; Hu et al., 2018). PCR-based approaches including digital PCR and droplet digital PCR (ddPCR) have been developed to detect ctDNA (Siravegna et al., 2017), however these methods are susceptible to false negatives and positives produced by interference from chemical species. Alternatively, DNA sequencing is a powerful tool for getting information of mutant status, but it requires expensive instrument and long turnaround time (Dewey et al., 2012). Therefore, developing inexpensive, quick and highly sensitive method for ctDNA mutation analysis remains a great challenge.

DNA as an attractive building material has been constructed various dynamic nanodevices including walkers (Chai and Miao, 2019; Jung et al., 2016), tweezers (Li et al., 2016; Peng et al., 2019), and nanorobots (Kopperger et al., 2018; Torelli et al., 2018) due to its programmable, addressable, and accurate Watson-Crick base pairing. Among them, intelligent DNA walkers have been extensively applied for biosensing (Yang et al., 2019; Zheng et al., 2018; He et al., 2017), bioimaging (Peng et al. 2017), and drug-delivery (Li et al., 2018a). In most case, the operation of DNA walkers is triggered by strand displacement reactions (Zheng et al., 2018), nicking enzymes

(Yang et al., 2016), and DNAzyme hydrolysis (Cha et al., 2015; Yang et al., 2018; Wang et al., 2018). For example, Liang developed entropy-driven DNA walker onto Au nanoparticle surfaces which can be actuated by additional fuel strand substrate (Liang et al., 2017). Fan et al. designed a stochastic DNA walker propelled by exonuclease III, which can selectively catalytic the removal of hybridized oligonucleotides (Qu et al., 2017). However, these walkers may confront with some challenges. First, DNA walkers needing supplement external substrates for continuous reaction tend to untimely stop operation in a local region of exhausted substrates (Jung et al., 2017). Second, leg DNA of the walkers may be prone to divorce from the preset track before hybridization with next neighboring substrate (Xu et al., 2019). Last, protein enzymes powered DNA walkers are hard to access substrates immobilized on nanoparticles or other sensing surfaces due to steric hindrance effect.

To address these difficulties, we successfully constructed a highly powered rolling walker for sensitive cfDNA analysis based on rolling circle amplification (RCA) with doxorubicin@tetrahedron functionalized gold nanoparticle (AuNP or Au) tags. Owing to ease of synthesis and high loading capacity, AuNPs are widely used to develop various biosensing platforms. However, the undesired aggregation or precipitation of AuNPs always happens in the test (Li et al., 2018b). DNA tetrahedron (TDN), an excellent nanoarchitecture with programmability and high loading capacity, is recently engineered as a significant paradigm for carrying numerous biomolecules (Wiraja et al., 2019). Thus, TDN is here properly employed as the nanocarrier to load doxorubicin (DOX) for forming DOX@TDN complex, which can further immobilize on AuNPs based on Au-S bond. The formed DOX@TDN-Au can not only enhance the dispersibility and solubility of AuNPs, but also offer an electrochemical indicator.

RCA is a powerful isothermal DNA replication tool which can autonomously synthesize a long single-stranded sequence with tandem repeats (Wang et al., 2015, Valero et al., 2018). By designing the circular template, thousands of periodic user-specified sequences can be produced in a single strand. Along with the operating progress, our multiple-legged walker system utilized the products of RCA as leg DNA, which gradually increased the binding power of the legs and the preset path to prevent

legs divorcing from the predefined track, because more and more legs irreversibly bind to substrates. In addition, all substrates of the rolling walker are immobilized on the sensing surface, without need of external dissociative strands for driving further walker locomotion. Moreover, the walker relies on strand displacement reactions rather than enzyme's cleavage to move, which avoided the steric hindrance effect. As we can see in the Scheme 1, Target binds to capture probe (CP) and ring, triggering RCA. The replicated DNA legs displace continuously the protruding domain (c) of iStep probes by strand displacement reactions, forming more stable dsDNA and guiding the motion of the walker along the path. As replication proceeds, the protruding domain (c) of iStep probes decrease gradually, which prevent DOX@TDN-Au tags from binding to sensing surfaces and producing electrochemical signal. On the contrary, there is a huge signal generated by the tags in the absence of the target.

2. Experiment section

2.1. Materials and reagents

All HPLC-purified oligonucleotide sequences displayed in Table S1 and chloroauric acid ($HAuCl_4$), 6-mercapto-1-hexanol (MCH), 10 mM dNTP mixture were synthesized by Sangon Biotechnology Co. Ltd (Shanghai, China). All oligonucleotides were dissolved in 1×TNaK buffer (20 mM Tris, 5mM KCl, 140 mM NaCl pH 7.5) and kept at -20 °C. T4 DNA ligase, Exonuclease I, Exonuclease III and Phi29 DNA polymerase were acquired from New England Biolabs (Beijing, China). Doxorubicin and GoldView were purchased from Solarbio science and technology co., Ltd (Beijing, China). The DNAs of clinical samples was kindly offered by the Affiliated Cancer Hospital of Chongqing University and approved by the medical ethics committee of the hospital (Chongqing, China). Clinical samples were mainly from puncture fluid and pleural effusion in patients with lung cancer. To get single-stranded DNA, the DNAs were heated to 95 °C for 5 min and then quickly cooled to 4 °C for 30 min before use. All other reagents were of analytical reagent grade. All aqueous solutions used in the experiments were prepared with Milli-Q

water (≥18 MΩ, Milli-Q, Millipore).

2.2. Apparatus

CHI660E electrochemical workstation obtained from Chenhua Instruments Co. Ltd (Shanghai, China) was employed in all electrochemical measurements. The gel electrophoresis experiment was carried out by using an Electrophoresis apparatus DYY-6C (Liuyi Instrument Company, China). Transmission electron microscope (TEM) (Hitachi-7500, Japan) and Atomic force microscope (AFM) Dimension Icon (Bruker AXS, Germany) were respectively utilized to characterize the size and morphology of gold nanoparticles and DNA tetrahedron nanostructure. The fabrication of Au-TDN@Dox was detected by UV-vis absorption spectra Nano-Drop1000 (Thermo, USA). The fluorescence signal was recorded by a Cary Eclipse fluorescence spectrophotometer (Agilent Technologies, U.S.A.).

2.3. Preparation of a circular template for RCA

The circular template (ring) was prepared by mixing circle probe (CiP) and primer at a ratio of 1:1.2, then annealed in a T100TM Thermal Cycler (Bio-Rad, U.S.A.). The following ligation reaction was conducted in a 20 μL reaction mixture containing hybridization complex (50 μM), 50 U T4 DNA ligase, 1× T4 DNA ligase buffer (50 mM Tris-HCl, 10 mM $MgCl_2$, 1 mM DTT and 1 mM ATP, pH 7.5). Ligation process was carried out at 16 °C overnight and following terminated by inactivation at 65°C for 10 min. Then, 40 U Exo I and 40 U Exo III were added to digest the leftover ssDNA and dsDNA to yield the closed circular template. After digestion, the Exo I and Exo III were further inactivated at 90°C for 20 min. The as-prepared circular template was then stored at -20°C for further use.

2.4. Preparation of DOX@TDN-Au tag

TDNs were synthesized by mixing equimolar quantities (100 μM) of four oligonucleotide strands (A, B, C and D) in TM buffer (20 mM Tris base, 50 mM $MgCl_2 \cdot 6H_2O$, pH 8.0). The mixed solution was heated to 95 °C for 5 min and then quickly cooled to 4 °C for 30 min in a T100TM Thermal Cycler (Bio-Rad, U.S.A.). The TDN solution was stored at 4 °C at least 5 h before use.

AuNPs were prepared according to the previous report (Liu et al., 2006). Briefly,

the $HAuCl_4$ solution (1 mM, 88.2 mL) was boiled in a 250 mL round-bottom flask with vigorous stirring, followed by the addition of trisodium citrate (34 mM, 10.1 mL) quickly. When the color changed from pale yellow to wine-red, the mixture was stopped heating and cooled to room temperature (RT) during stirring. The prepared AuNPs were stored at 4 °C in a brown glass bottle for further use.

The preparation of DOX@TDN-Au tag was illustrated as shown in Scheme 1. The mixture of TDN (25 μM, 320 μL) and the prepared AuNPs solution (1 mL) gently stirred at 25 °C overnight. Subsequently, 100 μL of PBS containing 1 M NaCl was added to the mixture stepwise to stabilize the obtained AuNPs probe. After that, 10 μL of DOX was added and stirred at 25 °C for 24 h for intercalating into double-stranded DNA. Then, the mixture was centrifuged and washed with PBS twice and resuspended in 1mL of PBS.

2.5. Surface modification of the Au-electrode

The bare Au-electrode was polished with 0.05 μm alumina powder to a mirror-like finish, followed by successive sonication in ultrapure water for a few minutes. After that, the Au-electrode was activated in newly prepared piranha solution (98% H_2SO_4: 30% H_2O_2, 3:1 by volume) for 5 min to eliminate other substances. The pretreated Au-electrode was rinsed with ultrapure water and dried in air. Then, 10 μL of 500 nM amine-modified probes (CP: iStep probes, 1:8 by volume) in binding buffer were added on the cleaned Au-electrode and incubated at 4 °C overnight. To obtain well-aligned DNA monolayer, the Au-electrode was incubated with MCH (10 μM, 10 μL) for 1 h at RT. Subsequently, the modified gold electrode was further used for detection of tumor DNA.

2.5. Electrochemical measurements

Initially, 10 μL of mixture consisted of target, ring and TNaK buffer was dropped on the prepared gold electrode and incubated at 37 °C for 0.5 h. After washed with the buffer, 10 μL of RCA system containing 0.2 U/μL Phi29 DNA polymerase, 200 μM dNTP, 100 ug/L BSA, 1 × phi29 DNA polymerase reaction buffer (500 mM Tris–HCl, 100 mM $MgCl_2$, 100 mM $(NH_4)_2SO_4$, and 40 mM DTT) was added and incubated at 37 °C for 1.5 h. Finally, 10 μL of DOX@TDN-Au suspension was further added on

the washed gold electrode and incubated at 37 °C for 0.5 h.

The electrochemical measurements were executed with a CHI 660C electrochemical analyzer in a three-electrode system, including a Pt wire as auxiliary electrode, an Ag/AgCl as reference electrode and a gold electrode as working electrode. The developed biosensor was measured by differential pulse voltammetry (DPV) from -0.3 V to -0.8 V with a scan rate of 50 mV/s in 0.1 M PBS (pH 7.0). Cyclic voltammetry (CV) (from -0.2 V to 0.6 V) and electrochemical impedance spectroscopy (EIS) were gained in 0.5 mM $[Fe(CN)_6]^{3-/4-}$ containing 0.1 M KCl, respectively.

3. Results and discussion

3.1. The design of rolling walker for electrochemical biosensing.

The principle of the target-driven rolling walker for electrochemical biosensing based on doxorubicin@tetrahedron-Au tag is illustrated in Scheme 1. The path on electrode consists of capture probe (CP) and iStep probes. Herein, the CP is designed for specifically recognition target and served as outset of the path. The iStep probe consists of three domains: a toehold domain (a), a double helix (b), and a protruding ssDNA domain (c) for hybridization of DOX@TDN-Au tag. The ring, acts as the rolling walker, is designed for rolling circle amplification (RCA), which produces a long and repetitive fragment to hybrid with domain a and domain b of iStep probe by toehold-initiated strand displacement.

In the absence of target, DOX@TDN-Au tags can attack to protruding ssDNA domain (c), which results in signal switch on. In the presence of target, the target specifically binds to CP (green portion) and ring (pink portion) respectively, resulting in generating a long single-stranded DNA containing tandem repeated sequences by RCA. The product of RCA can walk over to iStep probes, thus enabling binding to toehold domain (a) of iStep probe. Upon binding of iStep probe, the RCA product dissociates the hybridized double-stranded DNA via cascaded toehold-mediated strand displacement (TMSD), resulting in freeing the subunit (domain b^* and c) of iStep probe. In the process of RCA, the rolling walker remains binding to the

nanoengine and can be harnessed to guide the movement of the nanoengine along predefined walking tracks, resulting in continuous removal of subunit (domain b* and c) of iStep probes. Thus, Dox@TDN-Au tag cannot attack to iStep in the absence of protruding ssDNA domain (c), failing to produce output signal (signal off).

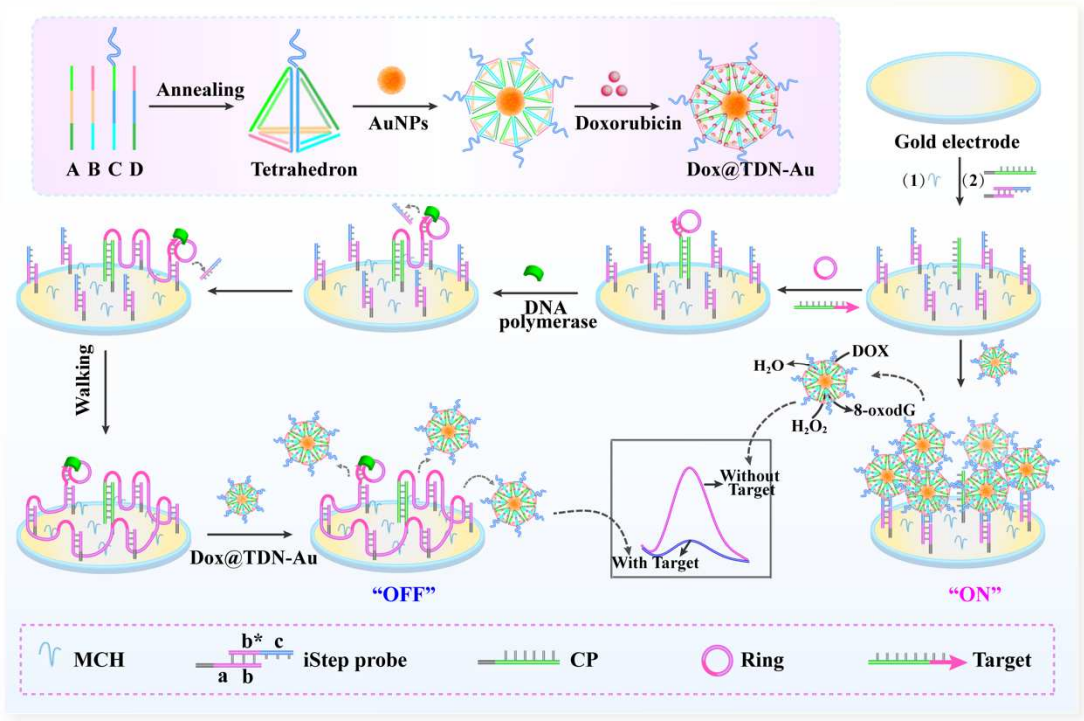

Scheme 1. Representation mechanism of the target-driven rolling walker for electrochemical biosensing based on DOX@TDN-Au tag. Arrows drawn on DNA strands represent 3′-termini.

3.2. Characterization of TDN

In order to characterize the formation of DNA tetrahedrons (TDN), atomic force microscopy (AFM) was applied for identifying their morphology. As shown in Figure 1A, one side of TDN was clearly seen. In Figure 1B, the height of TDN well matched with results in Figure 1A. To determine the synthesis process of TDN, native polyacrylamide gel electrophoresis (PAGE) was carried out for identifying their electrophoretic mobility. With the number of DNA strands increasing from A to D, the TDN bands migrated more slowly than other DNA combinations (Figure 1C). The integrity was further confirmed with Förster resonance energy transfer (FRET; Figure 1D). As shown in Figure 1D, strand A and B were labeled with Cy3 (donor) and Cy5

(acceptor), respectively. The formed TDNs could drive the dyes to proximity close enough for efficient FRET, resulting in a fluorescence decrease of Cy3 and increase of Cy5. The high FRET efficiency of formed TDNs was attributed to the rigidity and integrity of TDNs. These results indicated the successful synthesis of as designed TDN.

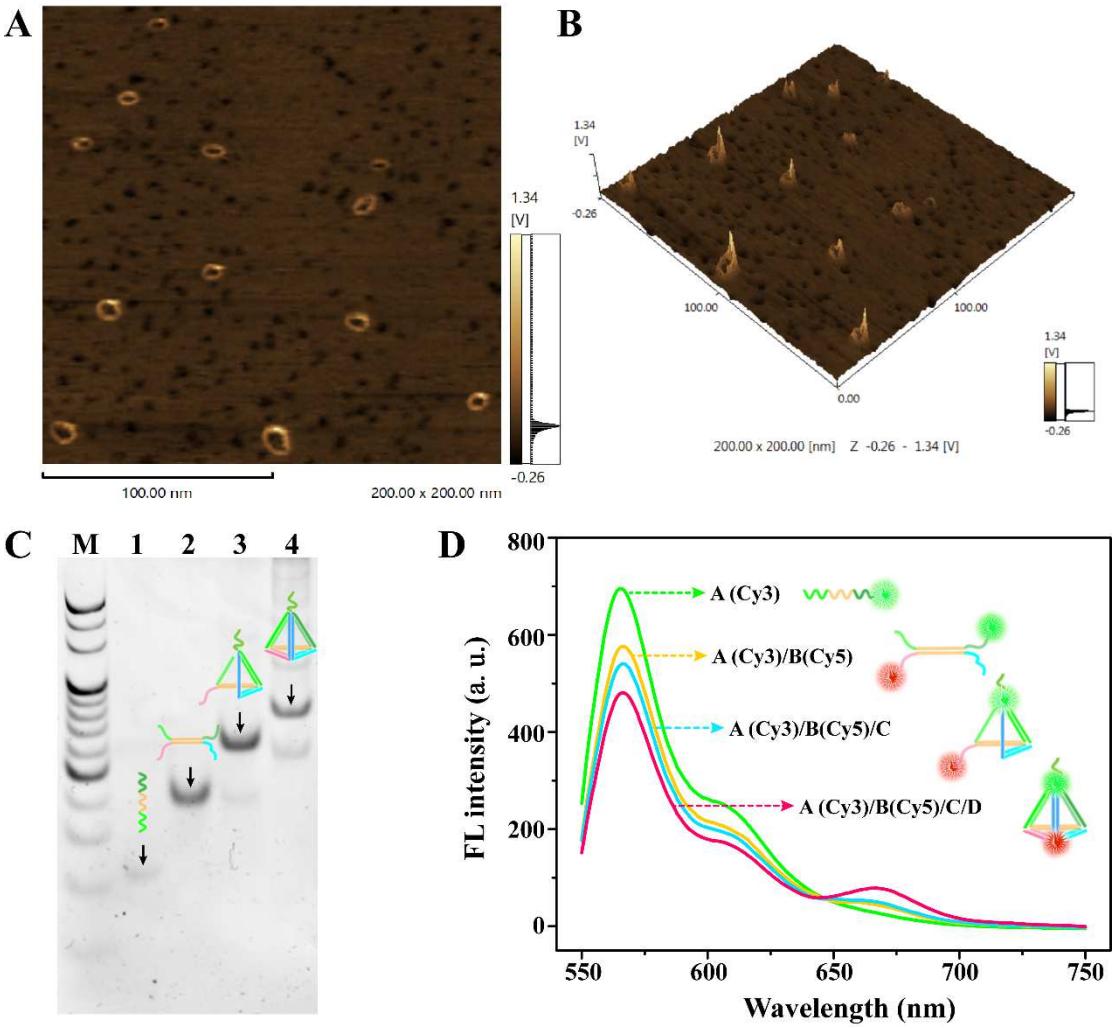

Figure 1 Characterization of TDN with AFM. Scale bar is 100 nm (A) and (B), native PAGE (C) and FRET (D) for characterization of TDN.

3.2. Characterization of AuNPs, TDN-Au and DOX@TDN-Au

Aiming to verify the synthesis of AuNPs and TDN-Au, TEM and DLS were carried out for identifying their morphology and size. The TEM images of the prepared AuNPs (Figure 2C) and TDN-Au (Figure 2D) showed they were both well-distributed, which were well matched with color change in the presence of 1 M

NaCl in Figure S2A. As seen in Figure 2A and 2B, the average diameter of AuNPs and TDN-Au were around 15 nm and 90 nm, respectively. To calculate the amount of TDN assembled on AuNP, the standard curve was gained with a series concentration of TDN (Figure S1A). Upon the fluorescence intensity of the supernatant containing excess TDN (Figure S1B), the amount of TDN on each AuNP was estimated to be about 72. Moreover, UV-vis spectra were further used for identifying the formation of the AuNPs, TDN-Au and DOX@TDN-Au. As seen in Figure S2A, the TDN-Au (b) and DOX@TDN-Au (c) were well dispersed in 1 M NaCl. However, the naked AuNPs were aggregated (d) in the presence of 1M NaCl. The UV-vis spectrum of Au-TDN showed the characteristic peaks of DNA at 260 nm and AuNPs at 522 nm. The TDN-Au (red) displayed a small red shift compared with unmodified AuNPs (black) at 519 nm (Figure S2B). The DOX@TDN-Au (pink) showed double peaks around 260 nm and widened peak at 500 nm. These results suggested the successful synthesis of DOX@TDN-Au.

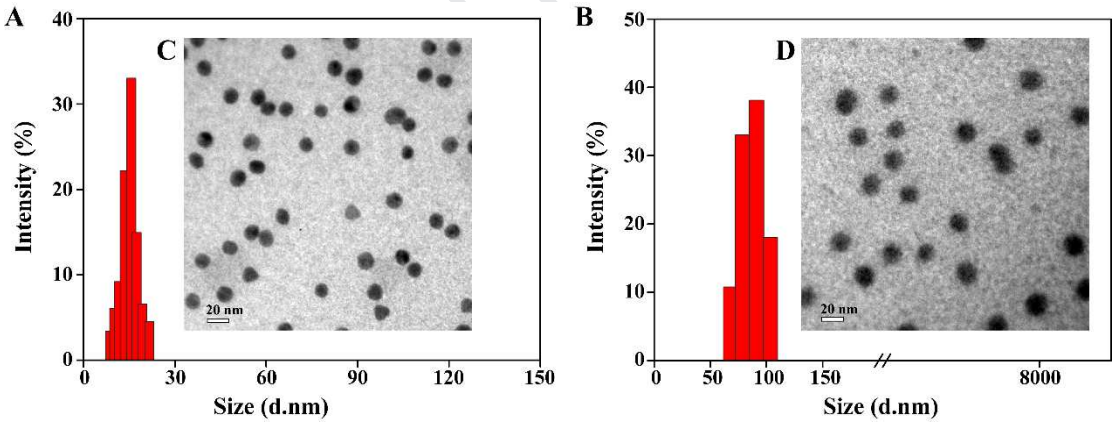

Figure 2 DLS characterization of the prepared (A) AuNPs and (B) Au-TDN. TEM image of the prepared (C) AuNPs and (D) Au-TDN.

3.3 Electrochemical characterization of the established biosensor

EIS and square wave voltammetry (SWV) measurements were applied to characterize the established electrochemical biosensor. The EIS curves were gained in 0.5 mM $[Fe(CN)_6]^{3-/4-}$ containing 0.1 M KCl and the semicircle diameter is equal to electron-transfer resistance (Ret). As Figure 3A shown, the bare Au electrode exhibited an almost straight line (curve a), which reflected the outstanding

electrochemical conductivity. After the thiolated CP and iStep probes were self-assembled onto the Au electrode, the Ret increased (curve b). When MCH were immobilized on the surface of Au electrode, the Ret increased obviously (curve c), attributing to the obstruction of the electron transfer. With the addition of target kras, the Ret increased slightly (curve d). Upon RCA, the Ret increased significantly (curve e and f), which suggested that the target initiated the RCA and a large amount of RCA products were generated. Afterwards, the remaining iStep probe hybridized with DOX@TDN-Au tags with participation of target kras, resulting in the slight decrease of Ret (curve f). Compared to curve f, the Ret decreased significantly in the absence of target (curve g), which was attributed to that the hybridization of iStep probe with DOX@TDN-Au could promote the electron transfer. These results were highly consistent with those gained from CV (Figure 3B) and SWV measurements (Figure 3C). In Figure 3C, the peak current with target decreased significantly compared to without target, and a remarkable peak shift in the current was 5.94 μA (red versus blue). Both results of EIS and SWV confirmed the truth of that the electrochemical biosensor worked indeed as described in the principle scheme.

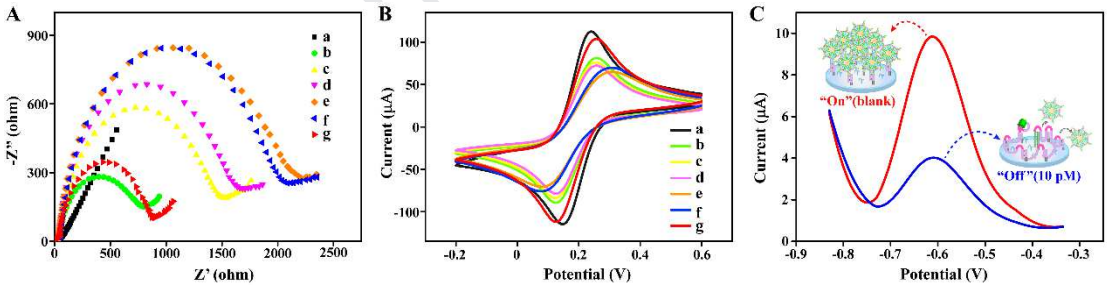

Figure 3 (A) EIS and (B) CV results of: (a) bare Au electrode, (b) a + CP + iStep probe, (c) b + MCH, (d) c + kras, (e) d + RCA, (f) e + Au-TDN@DOX, (g) c + Au-TDN@DOX. (C) Feasibility investigation of the electrochemical biosensor. DPV results: (red) with target (10 pM), (blue) blank. All data were obtained in Tris-HCl (20 mM, pH 7.4).

3.4. Native PAGE for characterization of target-driven rolling walker

A native PAGE experiment was carried out to characterize the feasibility of target-driven rolling walker (Figure S3). The primer, CiP and kras showed an obvious single band of DNA in lane 1, lane 2 and lane 5, respectively. Compared with the

band of DNA in lane 2, the band in lane 3 migrated much slower, indicating the formation of the ring. The presence of kras led to slightly slower migration of the ring (line 4), suggesting the hybridization of ring with kras. Upon RCA, a long ssDNA containing tandem repeated sequences was generated, resulting in the zero migration of the band (lane 6). After TMSD, the grayscale of band in lane 7 was obviously increased, indicating the hybridization of the products of RCA with iStep probe. These results successfully proved that the target could drive the rolling walker as described in Scheme 1.

3.5. Assay performance for kras detection

To obtain desirable analytical performance of the proposed assay, some experiment conditions were optimized, including incubation temperature, reaction time and the ratio of CP to iStep probe (Figure S4). The temperature was first optimized to be 37 °C (Figure S4A). At the optimal reaction temperature, the reaction time of RCA was evaluated. The current of blank (I_{blank})-to-I_{test} ratio achieved the maximum value at 90 min. Since the walking efficiency was firmly correlated with the ratio of CP to iStep probe, the CP-to-iStep probe ratio was finally examined. As shown in Figure S4C, the I_{blank}-to-I_{test} ratio gradually increased with the ratio from 1/1 to 1/8 and reached maximum value at 1/8. After that, the I_{blank}-to-I_{test} ratio experienced a decreasing trend. According to these optimal results, 37 °C, 90 min and the ratio of 1/8 for CP-to-iStep probe were used in the subsequent experiments.

To evaluate the sensitivity and dynamic range of the developed strategy, kras solutions with different concentrations were measured. As depicted in Figure 4A, the peak current decreased with the increase of kras concentrations, demonstrating that the failed attachment of signal tags to iStep was highly dependent on the concentration of kras. As shown in Figure 4B, the DPV responses exhibited a good linear relationship with the logarithmic value of kras concentration in the dynamic range from 1 fM to 10 nM. The obtained correlation equation was $Y = 4.658 – 0.874 \times \lg C$, with a correlation coefficient R^2 of 0.99, where C was the concentration of kras. The limit of detection (LOD) was calculated to be 0.29 fM based on the average signal of blank plus three times of the standard deviation. Compared to previous

reported methods for kras (Gao et al. 2018; Li et al. 2017b; Lu et al. 2016), the proposed sensing strategy achieved a superior or comparable sensitivity. Thus, this developed biosensor could be applied to quantification of kras with a wide linear range and low detection concentration.

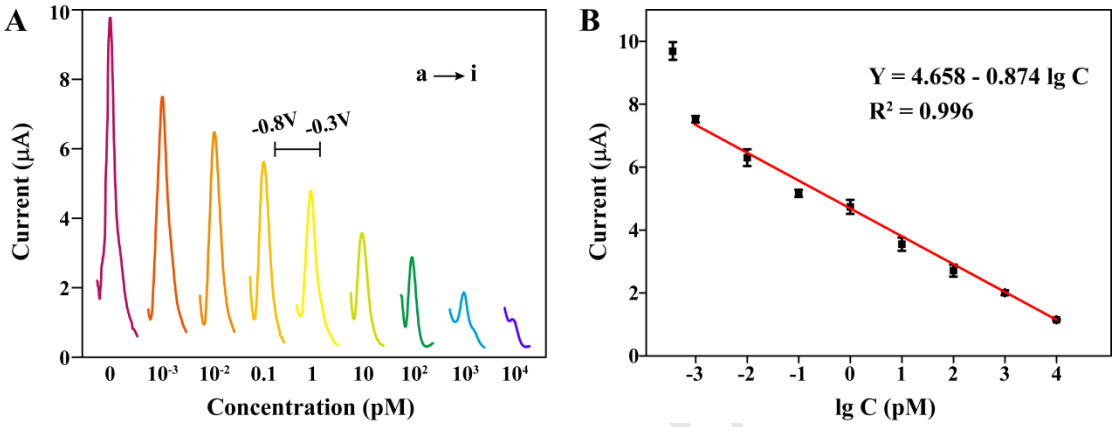

Figure 4 (A) DPV responses and (B) the corresponding calibration curve to various target concentrations (a to i: 0, 10^{-3}, 0.01, 0.1, 1.0, 10, 100, 10^{3} and 10^{4} pM). Error bars are standard deviation obtained from three independent experiments.

3.6. Specificity and reproducibility of the proposed biosensor

Specificity is crucial for sensing system. To evaluate the specificity of the constructed strategy, three different samples including mutant, wild type, and random sequence were detected under the same reaction conditions. As described in Figure 5A, a lowest DPV signal was obtained compared with the other two type sequence, and the shifts in the peak current were 9.19 μA (kras versus blank), 4.07 μA (wild type versus blank) and 2.58 μA (random sequence versus blank), respectively. In addition, the reproducibility of developed biosensor was further investigated by measuring the kras at 1 pM and 25 pM for five times. The relative standard deviations (RSD) for both concentrations were determined to be 2.75% and 3.62%. Therefore, the electrochemical biosensor was able to effectively detect the mutant gene with high specificity and acceptable reproducibility.

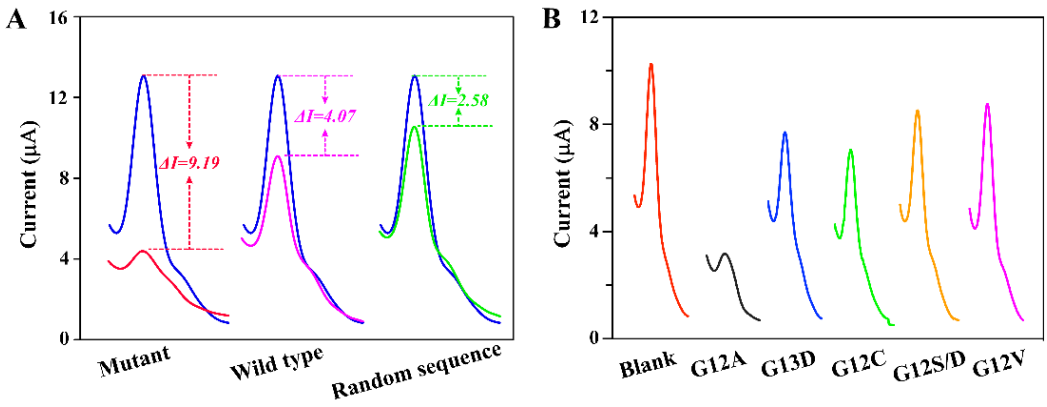

Figure 5 Specificity of the constructed strategy (A): current signal respectively corresponds to different genes: mutant, wild type, random sequence. "a" represent the control of blank. Clinical sample analysis (B): current signal respectively corresponds to different genes: blank, G12A, G13D, G12C, G12S/D, G12V. Error bars are standard deviation obtained from three independent experiments.

3.7. Real sample analysis

To validate the practicability of the proposed strategy for real sample analysis, the recoveries of different concentrations of kras in the diluted serum samples were detected with standard addition method. As shown in Table S2, the RSD was ranged from 2.6% to 3.1% and the recovery rate was from 96% to 106%, suggesting the acceptable analysis capability of the developed sensing method for real samples. In addition, the DNAs obtained from clinical samples were applied to investigate the practicability of the electrochemical sensor. As seen in Figure 5B, the current signal of kras (G12A) was significantly decreased compared with the other four mutant genes. Therefore, these results demonstrated that the developed biosensor held great potential in clinical applications.

4. Conclusion

In summary, we have successfully engineered a target-driven rolling walker for ultrasensitive electrochemical detection of ctDNA based on RCA with DOX@TDN-Au as signal tag. The developed biosensing method performed a low limit of detection (LOD) down to 0.29 fM and a wide dynamic detection range, which showed excellent specificity and a good performance in real sample analysis. Compared with the pre-reported works, this method has several prominent merits as

follows: (1) RCA powered DNA walkers are easy to attack to iStep probes immobilized on sensing surfaces with highly stability. (2) TDN functioned AuNPs endow the biosensor with highly stability and sensitivity. (3) Proximity-induced attacking of rolling walker on sensing surfaces ensures the developed method with excellent specificity. Therefore, our biosensing strategy exhibits enormous clinical translational value for point-of-care diagnostics owing to its high sensitivity, low background noise and rapid response ability.

Acknowledgements

This work was funded by the National Natural Science Foundation of China (81702083), Chongqing Basic Frontier Research (cstc2018jcyjax0132), and Chongqing Research Institute Performance Incentive Guidance Special Project (cstc2018jxjl130026).

References

Chan, K.C., Jiang, P., Zheng, Y.W., Liao, G.J., Sun, H., Wong, J., Siu, S.S., Chan, W.C., Chan, S.L., Chan, A.T., Lai, P.B., Chiu, R.W., Lo, Y.M., 2013. Clin. Chem. 59, 211-224.

Cha, T.G., Pan, J., Chen, H., Robinson, H.N., Li, X., Mao, C., Choi, J.H., 2015. J. Am. Chem. Soc. 137, 9429-9437.

Chai, H., Miao, P., 2019. Anal. Chem. 91, 4953-4957.

Das, J., Ivanov, I., Sargent, E.H., Kelley, S.O., 2016. J. Am. Chem. Soc. 138, 11009-11016.

Dewey, F.E., Pan, S., Wheeler, M.T., Quake, S.R., Ashley, E.A., 2012. Circulation 125, 931-944.

He, M.qi., Wang, K., Wang, W.J., Yu. Y.L., Wang, J.H., 2017. Anal. Chem. 89, 9292−9298.

Hu, P., Zhang, S., Wu, T., Ni, D., Fan, W., Zhu, Y., Qian, R., Shi, J., 2018. Adv. Mater. 30, 1801690.

Gorgannezhad, L., Umer, M., Islam, M.N., Nguyen, N.T., Shiddiky, M.J.A., 2018.

Lab Chip. 18, 1174-1196.

Jung, C., Allen, P.B., Ellington, A.D., 2017. ACS Nano. 11, 8047-8054.

Kamerkar, S., LeBleu, VS., Sugimoto, H., Yang, S., Ruivo, CF., Melo, S.A., Lee, J.J., Kalluri, R., 2017. Nature 546, 498-503.

Koldby, K.M., Mortensen, M.B., Detlefsen, S., Pfeiffer, P., Thomassen, M., Kruse, T.A., 2019. J. Gastroenterol. 54, 108-121.

Kopperger, E., List, J., Madhira, S., Rothfischer, F., Lamb, D.C., Simmel, F.C., 2018. Science 359, 296-301.

Li, D., Cheng, W., Li, Y., Xu, Y., Li, X., Yin, Y., Ju, H., Ding, S., 2016. Anal. Chem. 88, 7500-7506.

Li, S., Jiang, Q., Liu, S., Zhang, Y., Tian, Y., Song, C., Wang, J., Zou, Y., Anderson, G.J., Han, J.Y., Chang, Y., Liu, Y., Zhang, C., Chen, L., Zhou, G., Nie, G., Yan, H., Ding, B., Zhao, Y., 2018a. Nat. Biotechnol. 36, 258-264.

Li, X., Ye, M., Zhang, W., Tan, D., Jaffrezic-Renault, N., Yang, X., Guo, Z., 2019. Biosens. Bioelectron. 126, 596-607.

Li, X., Iocozzia, J., Chen, Y., Zhao, S., Cui, X., Wang, W., Yu, H., Lin, S., Lin, Z., 2018b. Angew Chem. Int. Ed. Engl. 57, 2046-2070.

Liang, C.P., Ma, P.Q., Liu, H., Guo, X., Yin, B.C., Ye, B.C., 2017. Angew Chem. Int. Ed. Engl. 56, 9077-9081.

Liu, J., Lu, Y., 2006. Nat. Protoc. 1, 246-252.

Peng, L., Yuan, Y., Fu, X., Fu, A., Zhang, P., Chai, Y., Gan, X., Yuan, R., 2019. Anal. Chem. 91, 3239-3245.

Peng, H., Li, X.F., Zhang, H., Le, X.C., 2017. Nat. Commun. 8,14378.

Qu, X., Zhu, D., Yao, G., Su, S., Chao, J., Liu, H., Zuo, X., Wang, L., Shi, J., Wang, L., Huang, W., Pei, H., Fan, C., 2017. Angew Chem. Int. Ed. Engl. 56, 1855-1858.

Siravegna, G., Marsoni, S., Siena, S., Bardelli, A., 2017. Nat. Rev. Clin. Oncol. 14, 531-548.

Speicher, M.R., Pantel, K., 2014. Nat. Biotechnol. 32, 441-443.

Sumbal, S., Javed, A., Afroze, B., Zulfiqar, H.F., Javed, F., Noreen, S., Ijaz, B.,

2018. Exp. Hematol. 65, 17-28.

Torelli, E., Manzano, M., Srivastava, S.K., Marks, R.S., 2018. Biosens. Bioelectron. 99, 209-215.

Jung, C., Allen, P.B., Ellington, A.D., 2016. Nat. Nanotechnol. 11, 157-163.

Valero, J., Pal, N., Dhakal, S., Walter, N.G., Famulok, M., 2018. Nat. Nanotechnol. 13, 496–503.

Wang, K, He, M.Q., Zhai, F.H., Wang, J., He, R.H., Yu Y.L., 2018. Biosens. Bioelectron. 105, 159-165.

Wang, L.D., Deng, R.J., Li, J.H., 2015. Chem. Sci. 6, 6777-6782.

Wiraja, C., Zhu, Y., Lio, D.C.S., Yeo, D.C., Xie, M., Fang, W., Li, Q., Zheng, M., Van Steensel, M., Wang, L., 2019. Nat. Commun. 10, 1147.

Yang, F., Zhong, X., Jiang, X., Zhuo, Y., Yuan, R., Wei, S., 2019. Biosens. Bioelectron. 130, 262-268.

Xu, Z., Chang, Y., Chai, Y., Wang, H., Yuan, R., 2019. Anal. Chem. 91, 4883-4888.

Yang, X., Tang, Y., Mason, S.D., Chen, J., Li, F., 2016. ACS Nano. 10, 2324-2330.

Yang, K., Wang, H., Ma, N., Zeng, M., Luo, H., He, D., 2018. ACS Appl. Mater. Interfaces 10, 44546-44553.

Zheng, J., Li, N., Li, C., Wang, X., Liu, Y., Mao, G., Ji, X., He, Z., 2018. Biosens. Bioelectron. 107, 40-46.

Zheng, J., Ji, X., Du, M., Tian, S., He, Z., 2018. Nanoscale 10, 17206-17211.

Highlights

1. A novel electrochemical biosensor was developed based on target-driven rolling walker with improved binding power of track for detection of circulating tumor DNA.
2. The rolling walker did not need addition of external strands to drive walking, for all walker components were immobilized on the sensing surface.
3. The movement of the multiple-legged walker was guided by strand displacement reactions, thus avoiding the steric hindrance effect brought by protein enzymes.
4. Doxorubicin@tetrahedron-Au was used as electrochemical signal tags.
5. The multiple-legged walker was performed in clinical samples with credible results.

Conflict of Interest

The authors declared that we have no conflicts of interest to this work.

Declaration of Interest Statement

We declare that we have no financial and personal relationships with other people or organizations that can inappropriately influence our work, there is no professional or other personal interest of any nature or kind in any product, service and/or company that could be construed as influencing the position presented in, or the review of, the manuscript entitled “Target-driven rolling walker based electrochemical biosensor for ultrasensitive detection of circulating tumor DNA using doxorubicin@tetrahedron-Au tags”.